

UTILIZING CMAQ PROCESS ANALYSIS TO UNDERSTAND THE IMPACTS OF CLIMATE CHANGE ON OZONE AND PARTICULATE MATTER

C. Hogrefe^{1,*}, B. Lynn², C. Rosenzweig³, R. Goldberg³, K. Civerolo⁴, J.-Y. Ku⁴, J. Rosenthal², K. Knowlton², and P.L. Kinney²

¹Atmospheric Sciences Research Center, State University of New York at Albany, ²Columbia University, ³NASA-Goddard Institute for Space Studies, ⁴New York State Department of Environmental Conservation

1. INTRODUCTION

Possible changes in O₃ and PM_{2.5} due to climate change are the result of a complex interplay of physical and chemical processes such as changes in chemical reaction rates, changes in biogenic emissions, and changes in transport patterns and mixing heights. The results presented in this paper build upon a recent study by Hogrefe et al. (2004a) who showed increased O₃ concentrations over the eastern United States in three future decades for a specific regional climate change scenario. In this paper, we expand upon this work by assessing the potential impact of climate change on PM_{2.5} concentrations. Furthermore, in an attempt to study the robustness of our results towards the choice of physics options in the MM5 regional climate model, CMAQ simulations were performed for two sets of MM5 configurations under both current and future climate scenarios. Finally, to study the relative contributions of various physical and chemical processes to simulated changes in pollutant concentrations, we utilized the integrated process rate (IPR) analysis feature contained in CMAQ.

2. MODEL DESCRIPTION AND DATA BASE

Emissions projections for greenhouse gases are used as inputs to the global and regional climate models to simulate future climate conditions. The Intergovernmental Panel On Climate Change (IPCC) Special Report on Emission Scenarios (SRES) describes various future emissions scenarios based on projections of population, technology change, economic growth, etc. In this paper, we utilize the greenhouse gas projections of the SRES A2 marker scenarios. The A2 scenario is one of the more pessimistic SRES marker scenarios and is

characterized by a large increase of CO₂ emissions (IPCC, 2000).

2.1 Emissions processing

As described in Hogrefe et al. (2004a,b), the county-level U.S. EPA 1996 National Emissions Trends (NET96) inventory processed by SMOKE was used as the basis for the air quality modeling presented in this study. Biogenic emissions were estimated by the Biogenic Emissions Inventory System – Version 2 (BEIS2). In the present study, the same anthropogenic emissions inventory and biogenic land use database was utilized for both the current and future climate simulations.

2.2 Global and regional climate modeling

Current and future year regional climate fields were obtained by coupling the MM5 mesoscale model (Grell et al., 1994) to the Goddard Institute for Space Studies (GISS) 4°x5° resolution Global Atmosphere-Ocean Model (GISS-GCM) (Russell et al., 1995) in a one-way mode through initial conditions and lateral boundaries. Simulations were performed for five consecutive summer seasons (June – August) in the 1990s and 2050s under the A2 climate scenario at a horizontal resolution of 36 km over the eastern United States. To test the sensitivity of air quality simulations towards uncertainties in the regional climate model, we utilized two sets of MM5 configurations for both decades. In one configuration, convective clouds were parameterized by the Betts-Miller scheme (Betts, 1986) and in the other configuration, the Grell scheme (Grell et al., 1994) was used. Hereafter, these two configurations are referred to as MM5-BM and MM5-G. Lynn et al. (2004, 2005) have shown that these two configurations simulate different spatial patterns of average temperatures, precipitation and clouds over the eastern U.S. for both the 1990s and 2050s. Furthermore, the spatial patterns and magnitude of changes in temperatures and other climate parameters also vary between the models, with the MM5-BM configuration typically predicting a larger degree of

* Corresponding author contact information: Christian Hogrefe, BAQAR, New York State Department of Environmental Conservation, 625 Broadway, Albany, NY 12233-3259, Phone (518) 402 8402, Fax (518) 402 9035, Email chogrefe@dec.state.ny.us

warming for the 2050s A2 scenario compared to the MM5-G configuration. However, it should be noted that the predictions of climate change from both MM5-BM and MM5-G lie within the span of climate predictions from several global models for the 2050s A2 scenario (Houghton et al., 2001). Therefore, these different configurations should be viewed as two members of a larger ensemble of possible future regional climate scenarios for the purpose of this study. Further details on the setup of this modeling system and results of the future regional climate simulations are described in Lynn et al. (2004, 2005).

2.3 Air Quality modeling

Using the processed emissions and the 36 km MM5 regional climate simulations for the five summer seasons in the 1990s and 2050s A2 scenarios, air quality simulations were performed using the Community Multiscale Air Quality (CMAQ) model (Byun and Ching, 1999) at a horizontal resolution of 36 km. The CMAQ evaluation results for simulating O₃ concentrations under present-day climate conditions have been presented in Hogrefe et al. (2004b). Time-invariant climatological profiles for O₃ and its precursors reflecting present day clean-air concentrations were used as boundary conditions (Byun and Ching, 1999). Details of the model setup are described in Hogrefe et al. (2004a,b). In this study, we included the aerosol and process analysis modules into the CMAQ simulations. Unless noted otherwise, we used CMAQ results over all non-water grid cells in the modeling domain except for a ring of 10 grid cells along the domain boundary for our analysis.

3. RESULTS AND DISCUSSION

Figure 1 shows the changes in summertime average surface level concentrations of total PM_{2.5} and its chemical components between the 2050s and 1990s. Results are shown for CMAQ driven by both the MM5-BM and MM5-G regional climate fields and indicate that total PM_{2.5} is predicted to increase for the 2050s climate scenario. Most of this increase is caused by an increase in sulfate aerosol, with a smaller contribution from increased elemental carbon and other unspciated fine particulates, both of them primary PM_{2.5} species that do not undergo chemical transformation within CMAQ. On the other hand, nitrate and organic carbon concentrations are predicted to decrease in the future climate scenario. While the magnitude of changes varies depending on the MM5 configuration utilized, the directionality of these

changes is consistent for all chemical components. The increase in sulfate concentrations is consistent with a more active photochemical regime indicated by higher temperatures and ozone concentrations reported for this climate scenario (Hogrefe et al., 2004a). Increased temperatures are also likely the cause for the decreases in nitrate and organic carbon concentrations since the gas/particle partitioning of these species is highly temperature-dependent. The increase of primary PM_{2.5} species points to changes in transport patterns and stagnation events since the concentrations of these species are governed solely by emissions (which are unchanged) and atmospheric transport and deposition. A recent study by Mickley et al. (2004) found increases in black carbon and CO over the eastern U.S. using a global-scale climate/chemistry model under the A1 climate scenario

In an attempt to identify causes for the changed concentrations of O₃ and PM_{2.5}, we employed the Integrated Process Rate (IPR) feature of CMAQ (Jeffries and Tonnesen, 1994; Byun and Ching, 1999). The purpose of IPR is to track the contribution of various physical and chemical processes to the hourly rates of change of pollutant concentrations. In the context of the present study, it is important to note that changes between concentrations in the current and future climate scenarios cannot be observed on an hour-by-hour basis because the meteorological regime for any given hour in the current climate does not correspond to the same meteorological regime for the same hour in the future climate case. Therefore, just as the effect of climate change on O₃ and PM_{2.5} concentrations was quantified by taking the differences of summertime average concentrations, the individual process rates from the two climate scenarios have to be aggregated both temporally and possibly spatially. Furthermore, for the present analysis, the individual process rates were aggregated to a horizontal term (sum of advection and diffusion), a vertical term (sum of advection, diffusion, mass adjustment, dry deposition, and emissions), a cloud term (including the effects of scavenging, aqueous phase chemistry and vertical cloud mixing), and a chemistry term (gas-phase or aerosol module chemical production and loss). In this study, we restricted our analysis to the first model layer only.

To illustrate the sign and strength of these four processes for several species, Figures 2a-e show these process rates averaged over all hours and all non-water non-boundary grid cells inside the

modeling domain for the 1990s and 2050s for O₃, SO₂, sulfate, nitrate, and elemental carbon. For O₃, the chemistry, horizontal, and cloud terms are all positive, while the net effect of all vertical processes is negative. The reverse is true of SO₂, consistent with the notion that SO₂ as a primary pollutant primarily from elevated point sources is mixed down to the surface from upper levels and consumed by both gas-phase and aqueous transformations. Figure 2d indicates that on a spatial and temporal average basis for the surface layer, the rate of change of nitrate formation is dominated by a positive contribution from vertical processes (including mixing and emissions) and a negative contribution from the aerosol module. Since elemental carbon is unreactive, there is no contribution from the aerosol module, while positive contributions from horizontal and vertical processes are balanced by negative contributions from cloud processes (cloud mixing and scavenging).

It should be noted that the signs and strengths of the processes discussed above exhibit both spatial and temporal variability. For example, the chemistry process rate for O₃ has its largest positive numbers in the southeastern U.S. and is negative in the vicinity of emissions-rich urban areas such as Chicago, Washington, D.C., and New York City. Likewise, chemical production rates for O₃ are positive during daytime at most locations and negative during nighttime. The results shown above are for the MM5-BM/CMAQ simulations only but are qualitatively similar for the MM5-G/CMAQ simulations.

For all of these components, the signs of the various processes do not change between the 1990s and 2050s, but the magnitude changes. For O₃, the magnitude of all processes increases, indicating a system where increased photochemical production is balanced by an increase in the strength of horizontal and vertical processes. In other words, these results indicate that, as the total integrated photochemical production of summertime O₃ over the domain increases, mixing and transport processes play an increased role in distributing ozone spatially. In contrast, the changes in process strengths for SO₂ and the PM_{2.5} components are relatively minor and have no uniform directionality. A possible reason for this behavior may be that changes in meteorological patterns and persistence play a bigger role in determining changes in average concentrations than any one of the individual processes investigated here. In particular, changes in chemical production/loss do not

appear to be the major driver of changes in these species.

In an attempt to find associations between the spatial patterns of changes in species concentrations, meteorological parameters, and various IPR terms, we constructed maps of changes in all of these variables between the 2050s and 1990s and then computed the cross-correlations between these maps. Table 1a shows correlations between the spatial patterns of concentrations changes and selected variables, while Table 1b shows correlations between the spatial patterns of meteorological changes and selected variables. The results in Table 1a illustrate that spatial patterns of summertime-average O₃ changes show moderate to strong correlations with spatial patterns of changes in CO and sulfate, while they are negatively correlated with the pattern of nitrate changes. The only O₃ IPR process whose spatial pattern of change shows a strong correlation with the spatial pattern of O₃ concentrations is chemistry with a correlation coefficient of 0.7. Similarly, the correlations between concentration changes in O₃, CO and sulfate appear to be attributable to similar spatial patterns of changes in their chemical production rates. Table 1b illustrates that spatial patterns of temperature changes are not a strong predictor of spatial patterns in concentration changes of O₃ or CO. However, there is a negative correlation between temperature changes and changes in EC, OC, other primary PM_{2.5}, ammonium and nitric acid. This negative correlation is also visible with spatial patterns of changes in PBL height, indicating that the rising temperatures might reduce the concentrations of these species through a combination of increased volatilization and increased PBL heights. Out of all meteorological variables, changes in water vapor show the strongest correlations with changes in O₃ and CO concentrations, possibly due to increased formation of HO_x radicals. Generally, the spatial patterns of change of most IPR processes show only weak correlation with the spatial patterns of changes of meteorological variables. The only exceptions are changes in chemical production for OC, CO, and to a lesser extent O₃ which show some correlations with changes in water vapor and/or temperature.

In summary, the results of the correlation analysis indicate that no single process factor or meteorological variable is sufficient to predict spatial patterns of changes in pollutant concentrations due to climate change. Even the strongest associations such as the mutual correlations between changes in temperature,

chemical production of CO, and concentrations of CO explain less than half of the concentration changes simulated by CMAQ. In other words, the resulting changes in pollutant concentrations are the result of a complex interaction between changes in transport, mixing and chemistry that cannot be parameterized by spatially uniform linear regression relationships. In the future, our analysis will be expanded to the full three-dimensional fields of meteorology, concentrations, and process rates.

4. SUMMARY

This paper described the application of a one-way coupled global/regional modeling system to simulate air quality in future decades over the eastern United States. Results indicate that climate change under the IPCC A2 emissions scenario for the 2050s is expected to cause an increase in summertime average total PM_{2.5} concentrations. Decreases in the volatile species nitrate and organic carbon are more than offset by increases in sulfate and primary PM_{2.5} species. In an attempt to study the robustness of these results towards the choice of physics options in the MM5 regional climate model, CMAQ simulations were performed with two sets of MM5 configurations under both current and future climate scenarios. While the spatial patterns of regional climate change and the magnitude of changes in pollutant concentrations show differences between the two sets of simulations, the directionality of concentrations changes was found to be robust towards the choice of physics options in the MM5 regional climate model. This finding implies that performing future regional climate ensemble modeling studies could help to quantify the uncertainty around simulated pollutant changes as a result of climate change. Results from CMAQ process analysis show that the strongest associations between climate change and changes in pollutant concentrations are found for chemical production rates of reactive species. However, even the strongest linear regression associations explain less than half of the concentration changes simulated by CMAQ. This implies that the simulated changes in pollutant concentrations stemming from climate change are the result of a complex interaction between changes in transport, mixing and chemistry that cannot be parameterized by spatially uniform linear regression relationships. Therefore, full-science photochemical modeling systems such as CMAQ are the tool of choice for studying the

impact of climate change on regional-scale air pollution.

5. ACKNOWLEDGMENTS

This work is supported by the U.S. Environmental Protection Agency under STAR grant R-82873301. Although the research described in this article has been funded in part by the U.S. Environmental Protection Agency, it has not been subjected to the Agency's required peer and policy review and therefore does not necessarily reflect the views of the Agency and no official endorsement should be inferred.

6. REFERENCES

- Betts, A.K., 1986: A new convective adjustment scheme. Part I: observational and theoretical basis. *Quart. J. Roy. Meteor. Soc.*, **112**, 677-692.
- Byun, D.W. and Ching, J.K.S. (eds.), 1999. Science algorithms of the EPA Models-3 Community Multiscale Air Quality Model (CMAQ) modeling system. *EPA/600/R-99/030*, U. S. Environmental Protection Agency, Office of Research and Development, Washington, DC 20460.
- Grell, G. A., J. Dudhia, and D. Stauffer, 1994: A description of the fifth-generation Penn State/NCAR Mesoscale Model (MM5). *NCAR Technical Note*, 138 pp., TN-398 + STR, National Center for Atmospheric Research, Boulder, CO
- Hogrefe, C., B. Lynn, K. Civerolo, J.-Y. Ku, J. Rosenthal, C. Rosenzweig, R. Goldberg, and P.L. Kinney, 2004a: Simulating changes in regional air pollution due to changes in global and regional climate and emissions, *J. Geophys. Res.*, Vol. 109, No. D22, D22301, 10.1029/2004JD004690.
- Hogrefe, C., J. Biswas, B. Lynn, K. Civerolo, J.-Y. Ku, J. Rosenthal, C. Rosenzweig, R. Goldberg, and P.L. Kinney, 2004b: Simulating regional-scale ozone climatology over the Eastern United States: Model evaluation results, *Atmos. Env.*, **38**, 2627-2638.
- Houghton, J. T.; Ding, Y.; Griggs, D.J.; Noguera, M.; van der Linden, P.J.; Dai, X.; Maskell, K.; Johnson, C.A., *Climate Change 2001: The Scientific Basis*, *Cambridge University Press*: Cambridge, **2001**, 892 pp.
- Intergovernmental Panel on Climate Change, 2000. *Special Report on Emissions Scenarios*. Nacenovic, N. and Swart, R. (eds.), *Cambridge University Press*, Cambridge, United Kingdom, 612 pp.

Jeffries, H.E., and S. Tonnesen, 1994: A comparison of two photochemical reaction mechanisms using mass balance and process analysis. *Atmos. Env.*, **28**, 2991-3003.

Lynn, B. H., L. Druyan, C. Hogrefe, J. Dudhia, C. Rosenzweig, R. Goldberg, D. Rind, R. Healy, J. Rosenthal, and P. Kinney, 2004: On the sensitivity of present and future surface temperatures to precipitation characteristics. *Climate Research*, **28**, 53-65

Lynn, B. H., C. Rosenzweig, R. Goldberg, C. Hogrefe, D. Rind, R. Healy, J. Dudhia, J. Biswas, L. Druyan, P. Kinney, and J. Rosenthal, 2005: The GISS-MM5 Regional

Climate Modeling System. Part I: Sensitivity of simulated current and future climate to model configuration. *J. Appl. Meteorol.*, in revision

Mickley, L.J., D.J. Jacob, B.D. Field, and D. Rind, 2004: Effects of future climate change on regional air pollution episodes in the United States, *Geophys. Res. Lett.*, **30**, L24103, doi:10.1029/2004GL021216.

Russell, G.L., J.R. Miller, and D. Rind 1995: A coupled atmosphere-ocean model for transient climate change studies. *Atmos.-Ocean* **33**, 683-730

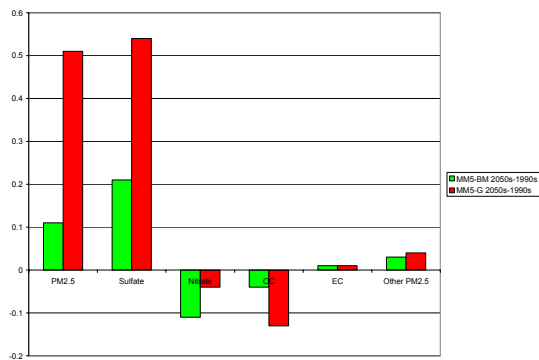


Figure 1: Changes in summertime average surface level concentrations of total PM_{2.5} and its chemical components between the 2050s and 1990s. These differences were calculated over all non-water grid cells in the modeling domain except for a ring of 10 grid cells along the domain boundary. Results are shown for CMAQ driven by both the MM5-BM and MM5-G regional climate fields.

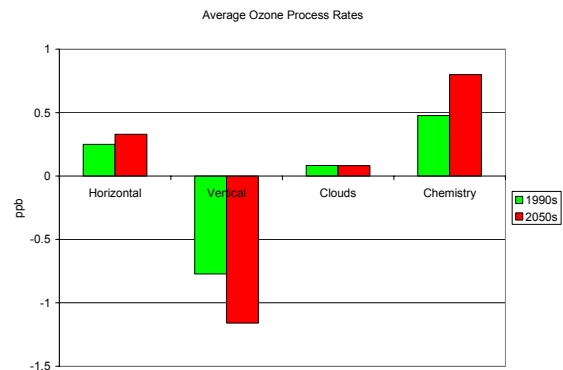


Figure 2a: O₃ process rates averaged over all hours and all non-water non-boundary grid cells inside the modeling domain for the 1990s and 2050s for the CMAQ simulations driven by the MM5-BM regional climate fields



Figure 2b: As in 2a, but for SO₂

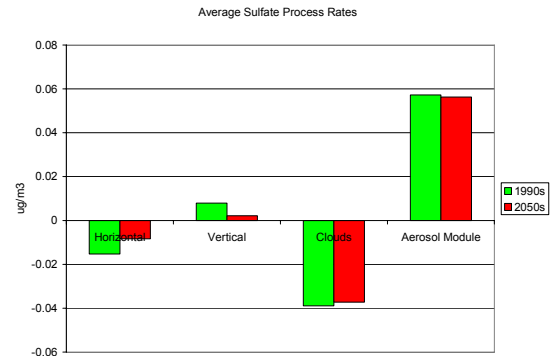


Figure 2c: As in 2a, but for Sulfate

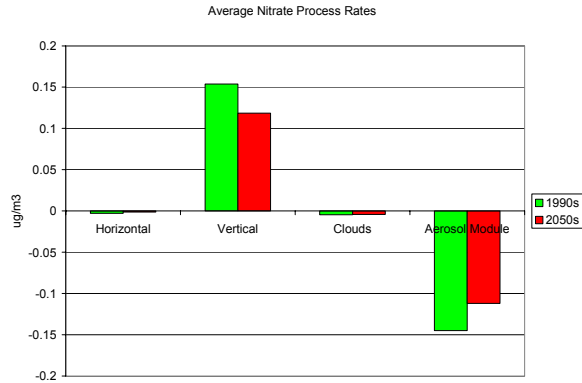


Figure 2d: As in 2a, but for nitrate

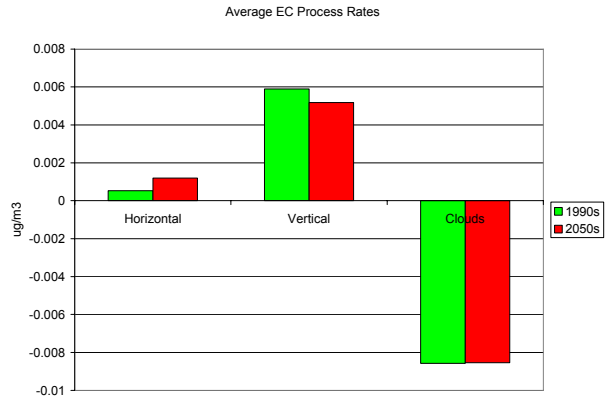


Figure 2e: As in 2a, but for EC

| | ΔCO | ΔO_3 | ΔEC | ΔSO_4 |
|--|-------------------|--------------------|-------------------|---------------------|
| ΔCO | 1.00 | 0.80 | 0.53 | 0.53 |
| ΔO_3 | 0.80 | 1.00 | 0.42 | 0.58 |
| ΔEC | 0.53 | 0.42 | 1.00 | 0.48 |
| $\Delta\text{Nitrate}$ | -0.30 | -0.56 | -0.10 | -0.27 |
| ΔOC | -0.05 | 0.05 | 0.60 | 0.27 |
| $\Delta\text{Sulfate}$ | 0.53 | 0.58 | 0.48 | 1.00 |
| $\Delta\text{IPR}(\text{EC}, \text{Clds})$ | -0.19 | -0.01 | 0.09 | -0.02 |
| $\Delta\text{IPR}(\text{EC}, \text{Hor})$ | 0.17 | 0.06 | 0.17 | 0.08 |
| $\Delta\text{IPR}(\text{EC}, \text{Ver})$ | -0.11 | -0.10 | -0.05 | -0.09 |
| $\Delta\text{IPR}(\text{SO}_4, \text{Chem})$ | 0.05 | 0.24 | 0.36 | 0.22 |
| $\Delta\text{IPR}(\text{SO}_4, \text{Clds})$ | -0.13 | -0.01 | 0.16 | 0.23 |
| $\Delta\text{IPR}(\text{SO}_4, \text{Hor})$ | 0.12 | -0.06 | -0.13 | -0.07 |
| $\Delta\text{IPR}(\text{SO}_4, \text{Ver})$ | -0.13 | -0.06 | 0.02 | -0.25 |
| $\Delta\text{IPR}(\text{CO}, \text{Chem})$ | 0.69 | 0.49 | 0.00 | -0.02 |
| $\Delta\text{IPR}(\text{CO}, \text{Clds})$ | -0.26 | -0.19 | -0.18 | -0.16 |
| $\Delta\text{IPR}(\text{CO}, \text{Hor})$ | 0.19 | 0.08 | 0.08 | 0.15 |
| $\Delta\text{IPR}(\text{CO}, \text{Ver})$ | -0.17 | -0.11 | 0.05 | -0.14 |
| $\Delta\text{IPR}(\text{O}_3, \text{Chem})$ | 0.57 | 0.70 | 0.37 | 0.31 |
| $\Delta\text{IPR}(\text{O}_3, \text{Clds})$ | 0.09 | -0.05 | 0.01 | 0.35 |
| $\Delta\text{IPR}(\text{O}_3, \text{Hor})$ | 0.10 | -0.03 | -0.10 | 0.09 |
| $\Delta\text{IPR}(\text{O}_3, \text{Ver})$ | -0.24 | -0.21 | -0.01 | -0.24 |
| $\Delta\text{IPR}(\text{SO}_2, \text{Chem})$ | -0.10 | -0.30 | -0.37 | -0.25 |
| $\Delta\text{IPR}(\text{SO}_2, \text{Clds})$ | -0.22 | -0.15 | 0.05 | -0.25 |
| $\Delta\text{IPR}(\text{SO}_2, \text{Hor})$ | 0.22 | 0.11 | 0.10 | 0.15 |
| $\Delta\text{IPR}(\text{SO}_2, \text{Ver})$ | 0.03 | 0.06 | 0.03 | -0.02 |
| $\Delta\text{CloudFraction}$ | 0.12 | -0.10 | -0.12 | 0.20 |
| ΔPBL | 0.09 | 0.04 | -0.32 | -0.21 |
| $\Delta\text{WaterVapor}$ | 0.60 | 0.48 | 0.00 | 0.10 |
| $\Delta\text{Temperature}$ | 0.08 | 0.01 | -0.35 | -0.28 |
| $\Delta\text{WindSpeed}$ | 0.13 | 0.07 | -0.35 | -0.02 |

Table 1a. Correlations between the spatial patterns of concentration changes between the 2050s and 1990s and changes in the spatial patterns for selected other variables. The spatial correlations were computed over all non-water grid cells.

| | ΔCF | ΔPBL | ΔWV | ΔT | ΔWSP |
|--|-------------------|--------------------|-------------------|------------------|--------------------|
| ΔCO | 0.12 | 0.09 | 0.60 | 0.08 | 0.13 |
| ΔHNO_3 | -0.27 | -0.28 | -0.04 | -0.33 | -0.38 |
| ΔO_3 | -0.10 | 0.04 | 0.48 | 0.01 | 0.07 |
| $\Delta\text{Ammonium}$ | 0.15 | -0.31 | -0.04 | -0.39 | -0.17 |
| ΔEC | -0.12 | -0.32 | 0.00 | -0.35 | -0.35 |
| $\Delta\text{Nitrate}$ | 0.10 | 0.01 | -0.19 | 0.00 | 0.03 |
| ΔOC | -0.08 | -0.63 | -0.52 | -0.53 | -0.49 |
| ΔA25 | -0.09 | -0.39 | 0.03 | -0.41 | -0.36 |
| $\Delta\text{Sulfate}$ | 0.20 | -0.21 | 0.10 | -0.28 | -0.02 |
| $\Delta\text{IPR}(\text{EC}, \text{Clds})$ | -0.29 | 0.02 | -0.27 | 0.02 | -0.31 |
| $\Delta\text{IPR}(\text{EC}, \text{Hor})$ | 0.19 | 0.07 | 0.11 | 0.05 | 0.14 |
| $\Delta\text{IPR}(\text{EC}, \text{Ver})$ | -0.20 | -0.01 | -0.14 | 0.05 | -0.11 |
| $\Delta\text{IPR}(\text{SO}_4, \text{Chem})$ | -0.31 | -0.23 | -0.19 | -0.23 | -0.34 |
| $\Delta\text{IPR}(\text{SO}_4, \text{Clds})$ | 0.03 | -0.25 | -0.21 | -0.26 | -0.25 |
| $\Delta\text{IPR}(\text{SO}_4, \text{Hor})$ | 0.14 | 0.29 | 0.10 | 0.30 | 0.15 |
| $\Delta\text{IPR}(\text{SO}_4, \text{Ver})$ | -0.24 | 0.02 | -0.12 | 0.10 | -0.11 |
| $\Delta\text{IPR}(\text{CO}, \text{Chem})$ | 0.05 | 0.47 | 0.78 | 0.46 | 0.34 |
| $\Delta\text{IPR}(\text{CO}, \text{Clds})$ | -0.05 | 0.11 | -0.17 | 0.10 | -0.10 |
| $\Delta\text{IPR}(\text{CO}, \text{Hor})$ | 0.29 | 0.10 | 0.08 | 0.09 | 0.11 |
| $\Delta\text{IPR}(\text{CO}, \text{Ver})$ | -0.26 | -0.02 | -0.23 | 0.04 | -0.15 |
| $\Delta\text{IPR}(\text{O}_3, \text{Chem})$ | -0.17 | 0.05 | 0.37 | -0.02 | -0.04 |
| $\Delta\text{IPR}(\text{O}_3, \text{Clds})$ | 0.39 | -0.17 | 0.04 | -0.26 | 0.21 |
| $\Delta\text{IPR}(\text{O}_3, \text{Hor})$ | 0.34 | 0.13 | 0.00 | 0.14 | 0.09 |
| $\Delta\text{IPR}(\text{O}_3, \text{Ver})$ | -0.19 | 0.03 | -0.25 | 0.10 | -0.08 |
| $\Delta\text{IPR}(\text{SO}_2, \text{Chem})$ | 0.30 | 0.21 | 0.15 | 0.21 | 0.32 |
| $\Delta\text{IPR}(\text{SO}_2, \text{Clds})$ | -0.35 | 0.07 | -0.30 | 0.08 | -0.33 |
| $\Delta\text{IPR}(\text{SO}_2, \text{Hor})$ | 0.28 | 0.06 | 0.15 | 0.05 | 0.13 |
| $\Delta\text{IPR}(\text{SO}_2, \text{Ver})$ | -0.20 | 0.02 | -0.03 | 0.08 | -0.04 |

Table 1b. Correlations between the spatial patterns of meteorological changes between the 2050s and 1990s and changes in the spatial patterns for selected other variables. The spatial correlations were computed over all non-water grid cells.